

Statistical Blockage Modeling and Robustness of Beamforming in Millimeter Wave Systems

Vasanthan Raghavan, Lida Akhoondzadeh-Asl, Vladimir Podshivalov, Joakim Hulten,

M. Ali Tassoudji, Ozge Hizir Koymen, Ashwin Sampath, and Junyi Li

Qualcomm Corporate R&D, USA,

Contact E-mail: vasanthan_raghavan@ieee.org

Abstract

There has been a growing interest in the commercialization of millimeter wave (mmW) technology as a part of the Fifth-Generation New Radio (5G-NR) wireless standardization efforts. In this direction, many sets of independent measurement campaigns show that wireless propagation at mmW carrier frequencies is only marginally worse than propagation at sub-6 GHz carrier frequencies for small-cell coverage — one of the most important use-cases for 5G-NR. On the other hand, the biggest determinants of viability of mmW systems in practice are penetration and blockage of mmW signals through different materials in the scattering environment. With this background, the focus of this paper is on understanding the impact of blockage of mmW signals and reduced spatial coverage due to penetration through the human hand, body, vehicles, etc. Leveraging measurements with a 28 GHz mmW experimental prototype and electromagnetic simulation studies, we first propose statistical blockage models to capture the impact of the hand, human body and vehicles. We then study the time-scales at which mmW signals are disrupted by blockage (hand and human body). Our results show that these events can be attributed to physical movements and the time-scales corresponding to blockage are hence on the order of a few 100 ms or more. Building on this fundamental understanding, we finally consider the broader question of robustness of mmW beamforming to handle blockage. Network densification, subarray switching in a user equipment (UE) designed with multiple subarrays, fall back mechanisms such as codebook enhancements and switching to legacy carriers in non-standalone deployments, etc. can address blockage before it leads to a deleterious impact on the mmW link margin.

Index Terms

A short version of this paper [1] has been submitted for publication to the IEEE International Workshop on Signal Processing Advances in Wireless Communications (SPAWC), Kalamata, Greece, 2018.

Millimeter wave, self-blockage, hand blockage, dynamic blockage, statistical modeling, beamforming, robustness, form-factor UE design

I. INTRODUCTION

The Fifth-Generation New Radio (5G-NR) wireless standardization efforts are an important component in the successful commercialization of millimeter wave (mmW) technology [2]–[5] for enhanced mobile broadband applications. In this direction, a number of (multi-institutional) efforts have focussed on the scope and scale of unfavorableness in wireless propagation at mmW carrier frequencies relative to sub-6 GHz systems [6]–[10]. These studies show that while propagation losses at mmW frequencies are typically higher than with sub-6 GHz systems in both indoor and outdoor settings, these losses are not¹ significantly worse at the mmW regime. These additional propagation losses can be overcome by array gains reaped from the use of larger antenna arrays (at both ends) [11]–[18], increased effective isotropic radiated power (EIRP) levels [19], and system design that aids in opportunistic signaling by leveraging time, frequency and space diversity [20]–[23].

Nevertheless, as the 5G-NR design process marches towards the accelerated schedule of early commercial deployments, important aspects that determine the viability of mmW technology in practice, such as outdoor-to-indoor penetration and blockage, have to be addressed carefully. Outdoor-to-indoor penetration through different types of residential/office materials has been studied extensively; see e.g., [9, Appendix E], [10]. These works report that the reflection response and penetration loss are a function of the material property, frequency, polarization and incident angle, and significantly deep signal reception notches spread over several GHz of the spectrum are observed. Such an observation motivates the need for system designs that support *both* frequency and spatial diversity.

In the context of spatial diversity, given the use of large antenna arrays and the diminishing beamwidths of the directional beams with antenna dimensions [15]–[18], mmW systems are

¹In particular, for non-line-of-sight (NLOS) links, [10] shows a nominal path loss degradation at 29 GHz relative to 2.9 GHz of 5.3 dB, 2.76 dB and 3.00 dB at a coverage distance of $d = 25$ m in an indoor office setting, $d = 200$ m in an Urban Micro setting, and $d = 100$ m in a shopping mall setting, respectively. This degradation is computed as $(\text{PLE}|_{29\text{ GHz}} - \text{PLE}|_{2.9\text{ GHz}}) \cdot 10 \log_{10}(d)$ dB at a coverage distance of d m where $\text{PLE}|_{29\text{ GHz}}$ and $\text{PLE}|_{2.9\text{ GHz}}$ denote the path loss exponent at the two carrier frequencies in the scenario of interest.

susceptible to signal blockage much more than sub-6 GHz systems are. In particular, mmW systems are susceptible to *self-blockage*, which is shadowing from the user itself in the form of hand blocking and blockage from other body parts. This can cause a complete blockage of the user equipment (UE) antennas depending on the antenna position relative to the hand. In addition, there are blockages from the environment around the UE in the form of buildings, foliage, or other obstructions (*static blockage*) and humans, vehicles, or moving obstructions (*dynamic blockage*).

Prior Work: In prior work, a human blockage model has been included in the 802.11(ad) 60 GHz wireless standardization efforts [8, Sections 3.3.8, 3.5.7, 5.3.9, 8]. This model captures the probability of a cluster blockage event and the distribution function of power attenuation for these events, both via ray-tracing studies. Wideband 60 GHz human blockage measurements over a 3 GHz bandwidth has been performed in [24] and the authors study the comparative model fits between the double knife edge diffraction (DKED) and the uniform theory of diffraction (UTD) modeling frameworks showing that the DKED framework underestimates blockage loss and the UTD framework overestimates it.

The Mobile and wireless communications Enablers for the Twenty-twenty Information Society (METIS) project has proposed a human blockage model based on the DKED framework in [9, pp. 39-41, 160-162]. A blockage model is proposed by the 3GPP Rel. 14 channel modeling document [6, pp. 53-57] for mmW system modeling under two variants: a stochastic variant (Option A) and a map-based variant (Option B). Both these variants assume a 30 dB flat loss for self-blockage. A modified version of the METIS model based on 73 GHz human blockage measurements using horn antennas has been proposed to account for directional transmissions in [7], [25], [26] and these studies show that human blockage could cause signal attenuation on the order of 30-40 dB depending on the distance between the human and the transmitter/receiver. Another work that studies UE antenna modeling in form-factor UE designs at 15 GHz from a blockage consideration is [27]. This study illustrates performance losses with the hand phantom model and recommends the use of subarray diversity to overcome these losses. The readers are pointed to [28], [29] for recent studies on design tradeoffs of 5G antenna arrays with form-factor considerations.

Contributions: With this backdrop, we first note that most of the prior works focus specifically on human blockers in a low-mobility indoor setting with short transmit-receive distances using

horn antennas for measurements. On the other hand, the use of a phased array (2-8 antennas) at the UE end implies that the beamwidth² at the UE side is expected to be much larger than that seen with a horn antenna. Such differences can lead to a significant variation between the blockage modeling experiments with a form-factor UE design and horn antenna measurements. In general, while form-factor UE design-based blockage modeling studies provide the *gold standard* in terms of understanding the implications of blockage at the UE end, such studies are currently difficult to obtain due to the still ongoing design, manufacture, development and testing of mmW technology supporting UEs/chipset solutions.

We propose to address these shortfalls by an intelligent mix of measurements with a form-factor UE prototype (as reported in [23]) and electromagnetic simulation studies for form-factor designs where such studies can supplant measurement-based insights. In particular, simulation studies are useful to understand the loss in spatial coverage with blockage. On the other hand, mmW measurements provide the best estimate for loss in signal strength as well as time-scales at which blockage disruptions happen. In this work, we provide a complementary mix of simulation studies and measurement studies for both self- and dynamic blockage.

In this direction, we first study self-blockage by considering electromagnetic simulations of antennas at 28 and 60 GHz in the proximity of the hand and identifying the spatial regions corresponding to signal blockage with different user grips. These simulation studies illustrate the blockage of a large spatial region in the UE's local coordinate system depending on whether the UE is held in a *Portrait* or *Landscape* mode. We then study the loss incurred by the hand with different grip experiments using the 28 GHz prototype reported in [23]. In contrast to prior work that shows high self-blockage losses (30 to 40 dB), our studies show that a median loss of 15 dB is incurred by the hand even in the most pessimistic scenario of a hard hand grip. The beamwidth differences between horn antennas and a phased array design is likely to account for such wide discrepancies.

To model dynamic blockage, we conduct simulation studies to capture the impact of objects at the UE end in the form of angular regions blocked and losses incurred with a DKED model. We study the efficacy of the simulated loss data with measurement studies using the 28 GHz

²For example, a beam with progressive phase shifts (or a constant phase offset) over a 4 element linear array is expected to lead to a 3 dB-beamwidth of $\approx 25^\circ$, whereas a horn antenna typically has a 3 dB-beamwidth on the order of 7.5° - 15° at mmW frequencies.

prototype. Our studies show that though there are some discrepancies between simulated loss and true measurements, simulated data can offer a reasonable first-order estimate of blockage losses and can thus be useful for scenarios like vehicular applications, where loss estimation with measurements is considerably more complicated and difficult. These studies lead to the proposal of a statistical blockage model that has many attractive properties: i) parsimonious (captured by a small number of model parameters), ii) efficacious (captures the real impact of blockages), and iii) computationally efficient (easily useable in a system simulator framework) in studying the performance of mmW systems.

We then consider the question of time-scales at which mmW signals are disrupted due to blockage. Such time-scale estimation is important to understand the scope of mmW beamforming solutions, their robustness/stability and the nature of mitigation mechanisms to handle blockage without serious link degradation. With some prototype studies, we show that these time-scales can be attributed to physical movements of the source of blockage (hand in the case of self-blockage, humans/vehicles in the case of dynamic blockage, etc.). Thus, the dynamics of these blockers capture the time-scales at which mmW signals get disrupted and measurement studies show that they are on the order of a few 100 ms (or more). Given the sub-ms (or a few ms) effective latencies targeted by 5G-NR for beam/subarray switching, it appears that the deleterious impact of blockages can be addressed by a robust beam management procedure at the PHY layer level. In terms of PHY layer solutions, network densification, design of multiple subarrays and capability to switch beams/subarrays at the UE end, and alternate fall back mechanisms could address these challenges.

Organization: This paper is organized as follows. Sections II and III consider self- and dynamic blockage from both electromagnetic simulation studies and measurement perspectives, and simple statistical models are proposed to capture the effect of these blockages. Section IV considers the question of time-scales at which blockage events happen. Section V proposes multiple approaches to combat the effect of blockages and Section VI concludes the paper.

II. SELF-BLOCKAGE

The focus of this section is on understanding the impact of self-blockage in terms of the spatial/angular coverage lost as well as the loss incurred over the blocked angles.

A. Loss in Spatial/Angular Coverage

Objects that are electrically small at microwave frequencies become electrically large at mmW frequencies, and small objects (which have the size of a few mm's) located in the proximity of the antennas affect the antenna performance and deteriorate both their efficiencies and radiation patterns. For example, antennas placed on the display side can be affected by the liquid crystal display (LCD) shielding, LCD glass, component shields, as well as other objects such as camera(s), speaker, microphone, sensors, etc.

To investigate the effect of the antennas' surroundings on its performance (especially its radiation pattern), the antenna module is placed over a simplified model of a UE (corresponding to a typical size of $60 \times 130 \text{ mm}^2$) and studied in an electromagnetic simulation framework. The model of the UE simulated consists of several layers of materials: Glass with a thickness of 1 mm, LCD shielding which lies beneath the glass and extends 15 mm from the edge of the glass, and the FR-4 board³ with a thickness of 0.8 mm that is separated by an 8 mm air gap from the LCD shielding. Also, a battery and few shielding boxes of random sizes are placed over the printed circuit board. All the metallic objects are connected to the ground plane of the board which covers its bottom plane.

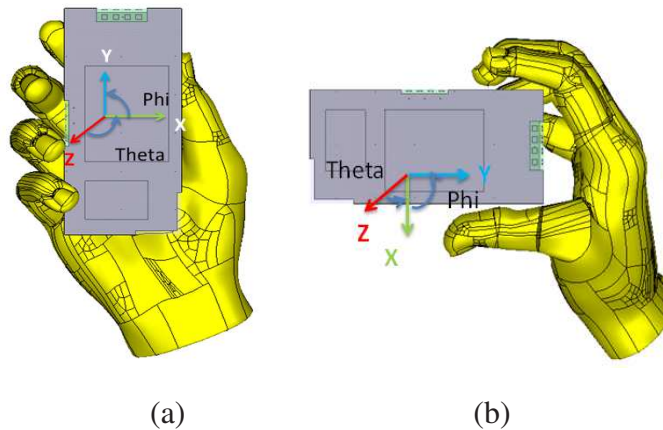


Fig. 1. A typical UE design with multiple subarrays and a hand phantom model in (a) *Portrait* mode and in (b) *Landscape* mode, along with the local coordinate system capturing azimuth and elevation angles (ϕ and θ).

³Note that “FR-4 (or FR4) is a grade designation assigned to glass-reinforced epoxy laminate sheets, tubes, rods and printed circuit boards. FR-4 is a composite material composed of woven fiberglass cloth with an epoxy resin binder that is flame resistant.” See <https://en.wikipedia.org/wiki/FR-4> for more details.

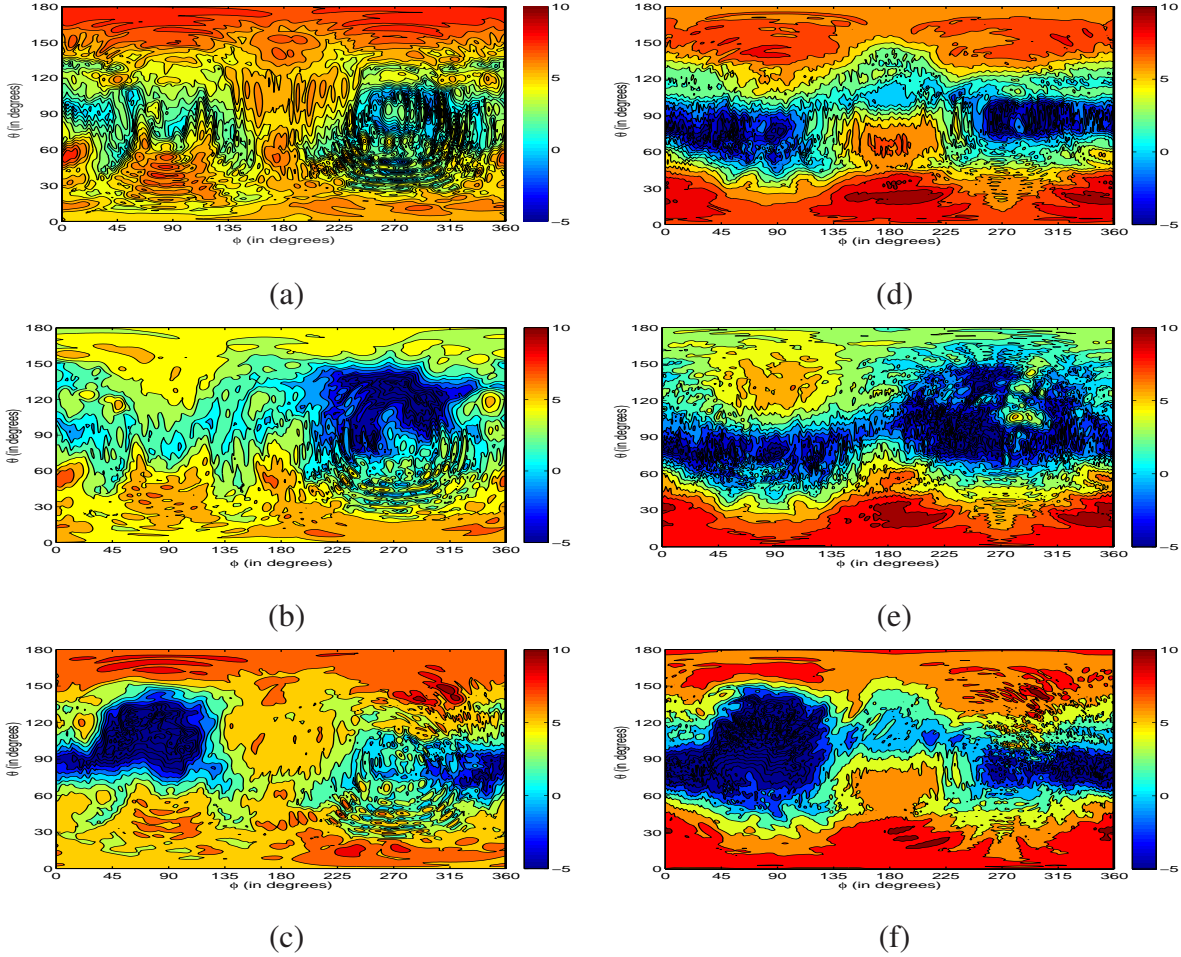


Fig. 2. Maximum gain of all antennas at 28 GHz: (a) No hand, (b) Hand in *Portrait* mode, (c) Hand in *Landscape* mode; and at 60 GHz: (d) No hand, (e) Hand in *Portrait* mode, (f) Hand in *Landscape* mode.

For the antenna design, multiple subarray units (corresponding to placement of antennas on the Long and Top edges of the UE) in the *Portrait* and in *Landscape* modes, as illustrated in Figs. 1(a)-(b), are considered. These antenna modules are designed on a relatively low loss dielectric substrate (Rogers 4003) and are placed on the FR-4 substrate. The antenna elements are either dipole elements or dual-polarized patch elements. Antennas are designed for the respective carrier frequency and are simulated with and without hand at every azimuth and elevation angle (ϕ and θ) in the spherical coordinate system.

To understand the impact of hand, the human hand is modelled as a homogeneous dielectric with the dielectric properties of skin tissue. In general, the skin permittivity decreases with an increase in frequency while its conductivity increases [30]–[32]. In particular, a relative dielectric

constant $\epsilon_r = 16.5$ and conductivity $\sigma = 25.8$ S/m are used at 28 GHz with CST Microwave Studio (a commercial electromagnetics simulation software suite). The hand dielectric properties determine the penetration depth into the hand and the reflection of electromagnetic waves from the hand. At the range of frequencies considered (28 and 60 GHz), the penetration depth into the hand is very small (corresponding to a high degree of reflection) ensuring a high degree of blockage by the hand.

The maximum gain of all the antennas without hand, with hand in the *Portrait* mode and with hand in the *Landscape* mode are plotted as two-dimensional contour plots (across ϕ - θ) in Figs. 2(a)-(c) for 28 GHz. From Fig. 2(a), in the absence of hand, almost the entire sphere is covered around the UE illustrating both the necessity and the goodness of the multi-subarray UE design. On the other hand, the presence of hand in either the *Portrait* or *Landscape* modes adversely affects the radiation coverage as seen from the blue areas⁴ (defined as signal strengths below -5 dBi) in Figs. 2(b)-(c). The region in blue stretches from behind the palm to the thumb (associated based on the corresponding ϕ - θ angles). Furthermore, it is seen that the long edge module does not play an important role in signal reception in the *Portrait* mode as it is blocked with the fingers resulting in significantly deteriorated antenna efficiencies. On the other hand, the short edge is not affected much with the presence of the hand ensuring that diversity from subarrays is critical for seamless communications. For the *Landscape* mode, the antennas along the long edge are unobstructed leading to better coverage than the short edge antennas.

While the electrical properties of the hand are different between 28 and 60 GHz, the hand still acts as a lossy reflector and can severely deteriorate antenna performance. In general, the skin permittivity and conductivity decreases and increases with frequency, respectively. Based on [30]–[32], a relative dielectric constant of $\epsilon_r = 7.9$ and conductivity of $\sigma = 36.4$ S/m are used at 60 GHz and simulations (as above) are redone. Figs. 2(d)-(f) plot the coverages without hand, with hand in the *Portrait* and *Landscape* modes, respectively, for 60 GHz. Compared to 28 GHz, at 60 GHz, the electrical size of the UE and hand are almost doubled while the antenna size is approximately reduced to half. This prevents the radiation of the antennas located on the top and left sides to leak to the right or bottom sides of the UE. Thus, even in the absence of hand, complete radiation coverage around the UE is quite challenging (as seen from the streaks

⁴Note that the heat map adjacent to the gain plots illustrate the strength of signal coverage.

of blue without the hand in Fig. 2(d)).

In the *Portrait* mode in Fig. 2(e), the left edge of the phone is obstructed by the fingers which causes blockage on the left side as well as back side of the hand. This forms a dead zone between 60° to 110° from the Z-axis, which is perpendicular to the hand. The high gain radiation coverage occurs in front of the phone due to radiation from the patch antennas located at the top edge. In comparison, the back of the phone which is illuminated by the top edge dipoles shows slightly lower gain. In the *Landscape* mode in Fig. 2(f), while neither subarray at the UE is blocked severely, the hand still prevents the top edge dipoles to radiate towards the back of the hand and most of the radiation is reflected or absorbed.

B. Loss in Signal Strength

The blockage loss incurred by the hand in the studies of Sec. II-A are plotted in Fig. 3(a) [see curves grouped as “Simulations”]. In particular, the cumulative distribution function (CDF) of the maximal gain from all the antennas in both polarizations is compared between the *Freespace* mode (without the hand) and *Portrait/Landscape* modes (with hand) and plotted here. These studies show that the loss appears to be in the range of -5 to 15 dB (with negative values corresponding to signal energy boosting due to hand reflection at certain angles). In particular, Fig. 3(a) shows that blockage loss is possible for up to 70% and 50% of the angles in *Portrait* and *Landscape* modes, respectively. However, these estimates are sensitive to the hand phantom model used in the simulation studies (see Fig. 1). In particular, the tightness of the hand grip around the UE determines what fraction of electromagnetic energy is captured by the antennas with a tighter/harder grip leading to significant losses (and *vice versa*). The nature of the air gap between the fingers also determines what fraction of energy is captured as multiple reflections from the skin surface, which can assist signal reception in certain angles. Thus, while the above simulation studies could be used for studying loss in angular coverage, using them directly for loss in signal strength could be questionable.

In this context, some measurement studies from [7], [25], [26] suggest a loss of even up to 30 to 40 dB with hand and body blockage. However, all these measurements are based on the use of horn antennas and cannot be extended easily to form-factor UE designs. To understand the loss possible with the hand, measurement studies are performed with a 28 GHz experimental prototype capturing the attributes of a 5G base-station as well as a form-factor UE design and

operating in a time-division duplexing framework. With this prototype, the baseband analog in-phase and quadrature (IQ) signals are routed to/from the modem to an IQ modulator/demodulator at 2.75 GHz center frequency. The 2.75 GHz intermediate frequency signal is translated to 28 GHz using a 25.25 GHz tunable local oscillator (with a 100 MHz step size). The base-station end of this system is a 16×8 planar array (made of a waveguide design) that allows analog beamforming using tunable four bit phase shifters and gain controllers. The UE end is a form-factor design made of four selectable subarrays, each a four element phased array of either dipoles or patches with locations on the UE as illustrated in Fig. 1(a). More details on the design parameters of the prototype are provided in [23].

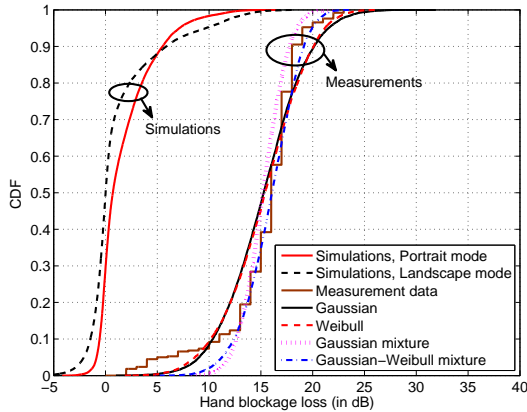
In our hand loss studies, the form-factor UE is grabbed by the hand at normal speed and the hand completely covers/envelops the active antenna arrays as illustrated in Fig. 3(b). All the subarrays at the UE side except the enveloped subarray are disabled in terms of beam switching thus allowing us to capture the blockage loss in terms of received signal strength differentials. We define an *RF event* relevant for these studies as one where the received signal strength indicator (RSSI) drops from the steady-state value by at least 2 dB. From our experiments, 38 such RF events are recorded and for each RF event, ten RSSI minimas⁵ spanning the entire event are separately recorded. The link degradation is computed as the RSSI difference between the steady-state RSSI value and the ten minimas. The empirical CDF of hand blockage loss corresponding to these 380 data points is also plotted in Fig. 3(a) [grouped under “Measurements”]. From this plot, we note that observations of 30-40 dB hand blockage loss from [7], [25], [26] may be too pessimistic to capture real measurements based on form-factor UE designs. More reasonable estimates for hand blockage loss are on the order of 5-20 dB with a median loss of 15 dB.

We now consider a number of model fits for the hand blockage loss data. The efficacy of each model (for the loss data) is captured by the Kolmogorov-Smirnov (KS) distance [33], defined as,

$$d_{KS}(\text{data}, \text{model}) \triangleq \max_x |F_{\text{data}}(x) - F_{\text{model}}(x)|,$$

where $F_{\text{data}}(x)$ and $F_{\text{model}}(x)$ denote the CDFs with the empirical data and the corresponding model, respectively. Since the KS distance only captures the worst-case deviation between the

⁵Due to constraints on the post-processing of data, RSSI minimas can be recorded to only within a 1 dB precision.



(a)



(b)

Fig. 3. (a) CDF of hand blockage loss with electromagnetic simulations using a hand phantom model, measurements using the experimental prototype, and model fits to measurement data. (b) Pictorial illustration of the hand holding experiment with the UE where the hand covers/envelops the active antenna array completely.

two CDFs, we also consider a data-weighted KS (WKS) distance, defined as,

$$d_{\text{WKS}}(\text{data}, \text{model}) \triangleq \int x \cdot |F_{\text{data}}(x) - F_{\text{model}}(x)| \cdot dx.$$

A better model fit for the data is captured by smaller KS and WKS distances (and *vice versa*).

TABLE I

MODEL FITS FOR HAND AND BODY BLOCKAGE LOSS

Model	Hand blockage			Body blockage		
	Parameters	d_{KS}	d_{WKS}	Parameters	d_{KS}	d_{WKS}
Gaussian: $\frac{1}{\sqrt{2\pi\sigma^2}} \cdot e^{-\frac{(x-\mu)^2}{2\sigma^2}}$	$\mu = 15.26, \sigma = 3.80$	0.19	1.22	$\mu = 8.54, \sigma = 2.45$	0.17	0.46
Weibull: $\frac{\beta}{\alpha} \cdot \left(\frac{x}{\alpha}\right)^{\beta-1} \cdot e^{-\left(\frac{x}{\alpha}\right)^\beta}$	$\alpha = 16.70, \beta = 4.61$	0.17	1.16	$\alpha = 9.43, \beta = 3.94$	0.16	0.45
Gaussian mixture: $\frac{p_1}{\sqrt{2\pi\sigma_1^2}} \cdot e^{-\frac{(x-\mu_1)^2}{2\sigma_1^2}} +$ $\frac{1-p_1}{\sqrt{2\pi\sigma_2^2}} \cdot e^{-\frac{(x-\mu_2)^2}{2\sigma_2^2}}$	$p_1 = 0.75, \mu_1 = 16.28,$ $\sigma_1 = 1.71, p_2 = 0.25,$ $\mu_2 = 12.15, \sigma_2 = 6.03$	0.26	1.51	$p_1 = 0.11, \mu_1 = 3.23,$ $\sigma_1 = 0.42, p_2 = 0.89,$ $\mu_2 = 9.17, \sigma_2 = 1.70$	0.21	0.62
Gaussian Weibull mixture: $\frac{p_1}{\sqrt{2\pi\sigma^2}} \cdot e^{-\frac{(x-\mu)^2}{2\sigma^2}} +$ $\frac{(1-p_1) \cdot \beta}{\alpha} \cdot \left(\frac{x}{\alpha}\right)^{\beta-1} \cdot e^{-\left(\frac{x}{\alpha}\right)^\beta}$	$p_1 = 0.15, \mu = 15.76,$ $\sigma = 3.55, p_2 = 0.85,$ $\alpha = 17.20, \beta = 6.11$	0.14	0.70	$p_1 = 0.15, \mu = 9.54,$ $\sigma = 1.95, p_2 = 0.85,$ $\alpha = 9.43, \beta = 3.69$	0.15	0.39

The empirical mean and empirical standard deviation of the hand blockage loss data are 15.26 dB and 3.80 dB, respectively. The functional forms as well KS and WKS distances of the different models considered here are presented in Table I. In terms of the models, we first consider a Gaussian density⁶ with mean and standard deviation being the empirical mean and empirical standard deviation values (as above). This model fit is plotted in Fig. 3(a). From this plot, we observe that the Gaussian density over-estimates both the lower and upper tail values of loss and under-estimates the bulk. That is, the measured data has a heavier lower tail than the Gaussian density can fit. This mismatch is also reflected in the high KS and WKS distances with this model (see Table I). To overcome this problem, we consider a Weibull density⁷ that is typically used to model heavy tailed data. While the Weibull density improves the KS and WKS distances, from Fig. 3(a) as well as Table I, we see that there is no dramatic improvement in fit with this model. Note that both these models are described by two parameters.

For a better fit, we therefore consider models with more parameters. While different model families can be considered, we start with a Gaussian mixture with the hope that these Gaussians can individually capture the upper and lower tails better. The parameters for the Gaussian mixture are learned using the Expectation Maximization algorithm as described in Appendix A. In contrast to the expectation, our results show that the best Gaussian mixture model fails to capture the data accurately as the tails of one Gaussian component lead to a poor fit for the other Gaussian component (and *vice versa*). In fact, the Gaussian mixture leads to a good fit only at the bulk. To remedy this misfit, we consider a Gaussian-Weibull mixture model as an alternate candidate. Since an analogous Expectation Maximization solution (as in Appendix A) appears to be difficult due to the complicated structure of the Weibull density, we use a local search over the parameter space neighborhood initialized with the individual Gaussian model and Weibull model parameters, respectively. The objective of this optimization is to minimize the WKS distance of the consequent model fit. As observed from both Fig. 3(a) and Table I,

⁶Theoretically, a Gaussian approximation to the loss can result in a value that is negative due to the Gaussian tail. Independent of whether negative loss values make sense, for all practical purposes, such realizations are not seen in numerical studies due to the extremely low probability of such occurrences. Thus, we will not bother with these technical difficulties in this paper.

⁷Note that the Weibull density $W(\alpha, \beta)$, where α and β are the scale and shape parameters, is commonly used to model “time-to-failure” of a certain process with β capturing the failure rate of the process. In particular, $\beta < 1$, $\beta = 1$ and $\beta > 1$ capture decreasing, constant, and increasing failure rates of the process with time.

the optimized Gaussian-Weibull mixture fits the empirical data better suggesting its utility as a generative model for hand blockage loss.

C. Proposed Statistical Model

Based on the studies in Sec. II-A and II-B, we propose a simple square region approximation for spatial/angular blockage with the hand. This approximation is captured by the center of the blocker (ϕ_1, θ_1) , and the angular spread of the blocker (x_1, y_1) in azimuth and elevation with the blocking angles captured as $\phi \in [\phi_1 - \frac{x_1}{2}, \phi_1 + \frac{x_1}{2}]$ and $\theta \in [\theta_1 - \frac{y_1}{2}, \theta_1 + \frac{y_1}{2}]$ in azimuth and elevation, respectively. For the blockage loss, we propose a low-complexity variant captured by the Gaussian fit and a relatively higher-complexity variant captured by the Gaussian-Weibull mixture fit from Table I. These proposals lead to the statistical model in Table II (in the local coordinate system around the UE) for self-blockage.

TABLE II
PROPOSED STATISTICAL MODEL FOR SELF-BLOCKAGE ($k = 1$)

Scenario	ϕ_1	x_1	θ_1	y_1	Blockage loss (in dB)
<i>Portrait mode</i>	260°	120°	100°	80°	Low-complexity : $\mathcal{N}(\mu = 15.3 \text{ dB}, \sigma = 3.8 \text{ dB})$
<i>Landscape mode</i>	40°	160°	110°	75°	High-complexity : Gaussian-Weibull mixture with $p_1 = 0.15, \mu = 15.8, \sigma = 3.6, p_2 = 0.85, \alpha = 17.2, \text{ and } \beta = 6.1$

III. DYNAMIC BLOCKAGE

A. Methodology for Modeling Dynamic Blockage

We assume that the dominant signal path(s) between the transmitter (base-station) and the receiver (UE) are in the plane connecting them. In outdoor use-cases where the transmitter is on the top of a building or a lamp post, as well as indoor use-cases where the transmitter is on/near the ceiling or at the same level as the receiver, such an assumption is reasonable⁸ with at least

⁸Nevertheless, this assumption significantly simplifies the study done in this work and should be treated as a first attempt at a comprehensive statistical model for blockage. Future studies will consider further extensions of the setup considered in this work.

moderate cell sizes. We now propose a simple methodology to capture the impact of dynamic blockers (e.g., humans, vehicles, etc.) that are strewn randomly in the transmit-receive plane.

Relative to a global coordinate system, the azimuth angle of the blockers are assumed to be uniform in $[0^\circ, 360^\circ)$ and the elevation angle is assumed to be a fixed θ_o . Without loss in generality, we assume that $\theta_o = 90^\circ$ (that is, the transmit-receive plane is the horizontal plane). If the blockers are too close to either the transmitter or the receiver, the observed blockage loss can be significant. At the receiver end, such a scenario is already captured by the self-blockage component and at the transmitter end, it is less likely provided the transmitter has a reasonable unobstructed coverage (the precise scenarios considered in this work).

To capture these aspects explicitly, as illustrated in the top-view of the transmit-receive plane in Fig. 4(a), the blockers are assumed to lie in a circular region (with radial locations r constrained as $d_{\min} \leq r \leq d_{\max}$) around the receiver. A triangular density function of the form

$$f(r) = \frac{2(r - d_{\min})}{(d_{\max} - d_{\min})^2}, \quad d_{\min} \leq r \leq d_{\max}$$

is assumed for r . This density captures the fact that the blocker density grows with r since there is more area covered by the circular region with r closer to d_{\max} than at d_{\min} . The heights and widths of the blockers are modeled as $h \sim \mathcal{U}([\bar{H} - h, \bar{H} + h])$ and $w \sim \mathcal{U}([\bar{W} - w, \bar{W} + w])$ where $\mathcal{U}([a, b])$ stands for a uniform random variable over the interval $[a, b]$, \bar{H} and \bar{W} denote the mean height and width of the blocker, and h and w denote the one-sided deviations for the height and width of the blocker, respectively.

We propose to model the number of blockers in the region of interest as a Poisson random variable with parameter λ . That is,

$$P(\text{No. of blockers} = k) = \frac{\lambda^k}{k!} \cdot e^{-\lambda}, \quad k = 0, 1, 2, \dots$$

Let the *average density of blockers* be defined as the number of blockers per unit area. With the model from Fig. 4(a), the average density of blockers is given as $\frac{\lambda}{\pi(d_{\max}^2 - d_{\min}^2)}$. For simplicity, the blocker and the receiver are assumed to be parallel in orientation and the angle subtended at the receiver/UE by the blocker is computed⁹ as $\sin\left(\frac{\phi}{2}\right) = \frac{w/2}{r}$ and $\sin\left(\frac{\theta}{2}\right) = \frac{h/2}{r}$ in azimuth and elevation, respectively.

⁹Since the distances tend to be small for both indoor and outdoor use-cases, approximations such as $\phi = \frac{w}{r}$ and $\theta = \frac{h}{r}$ can be inaccurate.

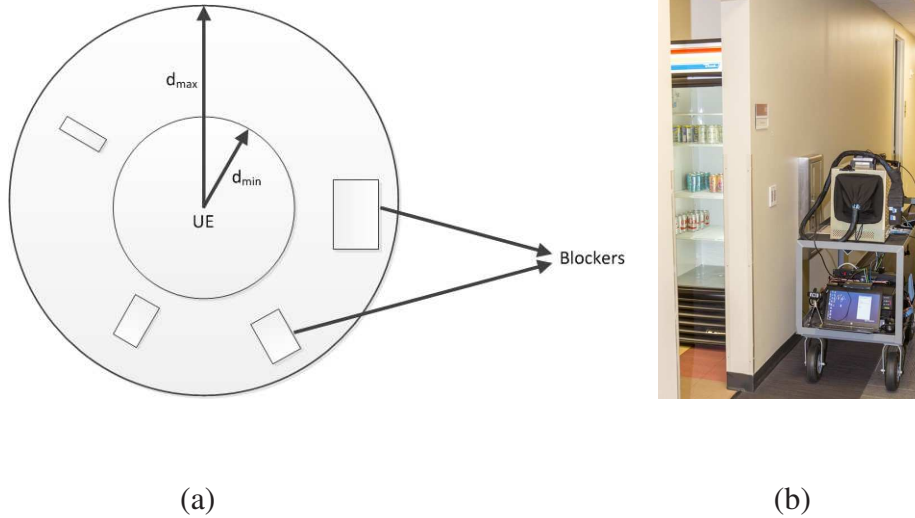


Fig. 4. (a) Top-view of simulation setup for studying dynamic blockage modeling. (b) Measurement scenario for body blockage studies.

TABLE III

AVERAGE DENSITY OF BLOCKERS WITH DIFFERENT d_{max} AND d_{min}

Human ($d_{min} = 3$ m)	$\lambda = 4$	$\lambda = 8$	$\lambda = 12$	Vehicular ($d_{min} = 5$ m)	$\lambda = 4$	$\lambda = 8$	$\lambda = 12$
$d_{max} = 10$ m	0.0140	0.0280	0.0420	$d_{max} = 30$ m	0.0015	0.0029	0.0044
$d_{max} = 15$ m	0.0059	0.0118	0.0177	$d_{max} = 40$ m	0.0008	0.0016	0.0024
$d_{max} = 20$ m	0.0033	0.0065	0.0098	$d_{max} = 50$ m	0.0005	0.0010	0.0015

To study the loss in spatial/angular coverage, we use the parameters from [7]: $\bar{H} = 1.7$ m and $\bar{W} = 0.3$ m for human blockers, and $\bar{H} = 1.4$ m and $\bar{W} = 4.8$ m for vehicular blockers. For modeling human and vehicular variations, we also use $h = 0.2$ m and $w = 0.1$ m for humans, and $h = 0.4$ m and $w = 0.5$ m for vehicles. In a typical indoor office setting such as the third floor of the Qualcomm building, Bridgewater, NJ with dimensions of 75×40 sq m and occupied by 50 to 100 humans, the average density of human blockers ranges from 0.0166 to 0.0333 per sq m. Similarly, in a typical outdoor setting of 100×100 sq m with 10 to 50 vehicles, the average density of vehicular blockers could range from 0.001 to 0.005 per sq m. For three choices of λ and d_{max} , Table III presents the average density of human and vehicular blockers in the indoor

and outdoor cases, respectively. For a human blocker, we assume $d_{\min} = 3$ m and three cases for d_{\max} : $d_{\max} = 10, 15,$ or 20 m (denoted as Cases 1-3). For a vehicular blocker, we consider $d_{\min} = 5$ m and three cases for d_{\max} : $d_{\max} = 30, 40,$ or 50 m (also denoted as Cases 1-3). While different choices of λ can be considered in general, from Table III, we focus on $\lambda = 4, 8, 12$ as representative samples to reflect average density of blockers in typical indoor and outdoor deployments.

B. Loss in Spatial/Angular Coverage and Number of Blockers

Table IV presents the median, 90th and 95th percentile values of the mean angular blockage in azimuth and elevation for $\lambda = 4, 8$ and 12 . From these studies, we note that the mean spatial/angular blockage for both human and vehicular blockers decreases as d_{\min} increases or d_{\max} increases. This is because the blockers are farther away from the receiver as d_{\min} increases and are more likely to be farther away from the receiver as d_{\max} increases. In either case, a smaller angle is casted at the receiver leading to a reduction in the mean angular blockage. Further, this angle has only a weak dependence on λ . We conclude that a typical mean angular blockage of 2.5° in azimuth and 15° in elevation are seen with human blockers, and 15° in azimuth and 5° in elevation are seen for vehicular blockers.

We are now interested in understanding the number of blockers K to be incorporated in a statistical model for dynamic blockage. Table V presents the explanatory power captured by the fraction of the total azimuthal angular blockage captured¹⁰ by the top- K blockers. The median, 90th and 95th percentile values of the explanatory power are presented for human blockers with $d_{\min} = 3$ m, $d_{\max} = 15$ m, and for vehicular blockers with $d_{\min} = 5$ m, $d_{\max} = 40$ m for different choices of λ . Table V shows that there is a decreasing explanatory power for a fixed K as λ increases, and diminishing returns and increasing model complexity with an increase in K for any λ . The use of the top-4 human and top-3 vehicular blockers can explain over 60% of the blocked angular region up to $\lambda = 8$ and suggests a good tradeoff point/compromise between explanatory power and model complexity.

¹⁰While we consider the top- K blockers in terms of angles blocked, alternate criteria such as top- K blockers in terms of blockage loss can also be considered. The flavor of the results are not expected to change with such alternate criterion.

TABLE IV

ANGULAR BLOCKAGE METRICS WITH HUMAN AND VEHICULAR BLOCKERS

		Mean angular blockage (Human)						Mean angular blockage (Vehicular)					
		Azimuth (in degrees)			Elevation (in degrees)			Azimuth (in degrees)			Elevation (in degrees)		
Percentiles		50	90	95	50	90	95	50	90	95	50	90	95
$\lambda = 4$	Case 1	2.34	3.00	3.26	13.19	16.34	17.55	14.27	20.50	23.14	4.02	5.71	6.41
	Case 2	1.65	2.24	2.48	9.31	12.32	13.54	10.80	16.00	18.31	3.07	4.53	5.19
	Case 3	1.28	1.80	2.03	7.21	9.95	11.10	8.74	13.14	15.19	2.50	3.78	4.36
$\lambda = 8$	Case 1	2.40	2.88	3.05	13.44	15.57	16.32	15.69	20.98	23.06	4.25	5.54	6.03
	Case 2	1.71	2.11	2.26	9.60	11.62	12.37	11.79	15.88	17.47	3.27	4.37	4.81
	Case 3	1.33	1.69	1.83	7.47	9.36	10.10	9.48	12.81	14.18	2.66	3.63	4.02
$\lambda = 12$	Case 1	2.44	2.84	2.98	13.55	15.29	15.84	16.90	22.04	24.07	4.42	5.55	5.95
	Case 2	1.73	2.07	2.18	9.69	11.33	11.89	12.50	16.24	17.65	3.38	4.34	4.69
	Case 3	1.35	1.64	1.74	7.56	9.07	9.60	9.95	12.93	14.07	2.75	3.58	3.90

TABLE V

EXPLANATORY POWER OF THE TOP- K BLOCKERS

		$\lambda = 4$			$\lambda = 8$			$\lambda = 12$		
Percentiles		50	90	95	50	90	95	50	90	95
Human	Top-2	64.54%	42.16%	38.04%	39.12%	27.66%	25.31%	29.37%	21.45%	19.78%
	Top-3	84.51%	58.44%	53.04%	53.42%	38.88%	35.72%	40.41%	30.28%	28.15%
	Top-4	100.00%	72.89%	66.16%	65.96%	48.86%	45.14%	50.20%	38.26%	35.75%
	Top-5	100.00%	86.06%	78.09%	77.27%	57.93%	53.83%	59.06%	45.65%	42.76%
	Top-6	100.00%	100.00%	89.36%	86.94%	66.32%	61.85%	67.18%	52.50%	49.29%
Vehicular	Top-2	70.18%	46.48%	42.12%	47.48%	34.30%	31.51%	39.44%	29.14%	26.96%
	Top-3	100.00%	64.17%	58.18%	63.33%	47.59%	44.08%	52.94%	40.67%	37.86%
	Top-4	100.00%	78.23%	72.42%	76.34%	59.02%	55.08%	64.28%	50.82%	47.56%
	Top-5	100.00%	89.72%	85.90%	88.29%	69.22%	64.86%	73.97%	59.78%	56.24%
	Top-6	100.00%	100.00%	100.00%	100.00%	78.26%	73.72%	79.79%	64.93%	61.52%

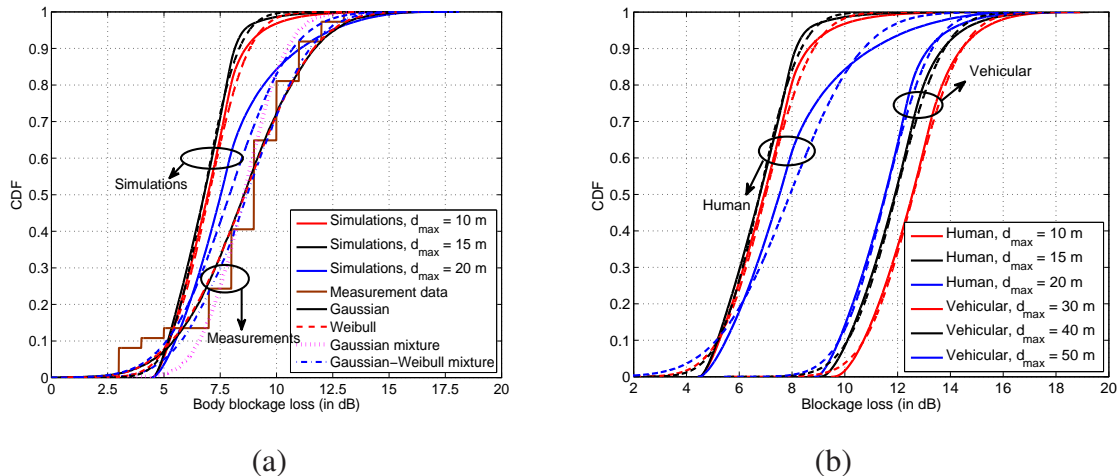


Fig. 5. (a) CDF of human body blockage loss with simulations using the dynamic blockage methodology, measurements using the experimental prototype, and model fits to measurement data. (b) CDF of human body and vehicular blockage loss with simulations using the dynamic blockage methodology.

C. Loss in Signal Strength

For the human body blockage loss, we use the DKED model from [7], [34], [35] with $d_{\min} = 0.5$ m, $\lambda = 4$ and the transmit-receive distance $R = 20.5$ m. Fig. 5(a) plots the CDF of the body blockage loss (solid curves) with different choices of d_{\max} . Also, plotted are Gaussian approximations to the loss estimated from the DKED model (dashed curves). While blockage losses increase as the blockers get close to either the transmitter or receiver, the Gaussian approximation appears to be a reasonable first-order fit across different choices of d_{\max} .

Nevertheless, these losses are sensitive to the assumptions in the simulation methodology described in Sec. III-A. Thus, analogous to the measurements reported in Sec. II-B, link reliability studies are conducted in the third floor of the Qualcomm building, Bridgewater, NJ with the experimental prototype described in Sec. II-B to understand the impact of (human) body blockage. In these experiments, as illustrated in Fig. 4(b), the UE side of the prototype is held stationary near the vending machine(s). The UE antenna height is adjusted to 1 m with possible transmission (over an NLOS link) from one of two transmitters. One of these transmitters is at a distance of ≈ 20 m from the UE and the other is at a distance of ≈ 40 m. Both transmitters are held stationary and are maintained at a height of 2 m. Except for one active subarray, beam

switching across different subarrays is disabled. Uncontrolled tests are performed where people could walk by/past the UE at normal pedestrian speeds and at different distances (people could get as close as 0.5 m from the UE).

The body blockage loss¹¹ corresponding to 111 RF events with humans blocking the UE are recorded and the CDF of this loss data is also presented in Fig. 5(a). The empirical mean and empirical standard deviation for the loss data are 8.54 dB and 2.45 dB, respectively. As with the self-blockage studies, the same set of four models (considered earlier) are fitted to the body blockage loss data. The parameters learned in this process as well as the KS and WKS distances between the empirical data and the fitted models are presented in Table I. From this study, we note the best fit for the data again with a Gaussian-Weibull mixture.

From Fig. 5(a), we observe that there exists a minimal yet distinct difference between the loss estimated from simulation studies and those with measurements. As mentioned earlier, these differences arise from the failure of the simulation methodology to capture real deployment scenarios and addition of more details could bridge this gap. This would be the subject of future investigations. Nevertheless, given the lack of/difficulty in obtaining measurements in outdoor scenarios, the simulation methodology described in Sec. III-A is considered for vehicular blockers with $d_{\min} = 5$ m, $\lambda = 4$ and $R = 100$ m. From this study, Fig. 5(b) presents a comparison between human and vehicular blockers in terms of simulation studies. Typical median losses of 6.5 to 8 dB and 11.5 to 12.5 dB are seen in the human and vehicular cases, respectively. These studies illustrate the far more significant impact vehicular blockers could have in real deployments than human blockers making the understanding of such issues more important.

D. Proposed Statistical Model

Table VI summarizes the main conclusions of the studies in Sec. III-B and III-C in terms of the number, center and angular spread, and loss due to both human and vehicular blockers. While a measurements-driven loss model is proposed for human body blockage, only a simulations-based loss model (developed based on the proposed methodology in Sec. III-A) is available for vehicular blockage. A similar model is proposed by 3GPP to capture blockage effects [6, pp. 53-55]. The 3GPP model differs from the proposal in Table VI in terms of the number of blockers

¹¹As in the self-blockage studies, RSSI could be recorded to only within a 1 dB precision.

and their blockage regions. Further, while a *low-complexity* statistical version of the DKED model is proposed for vehicular blockage in Table VI, a more explicit version is proposed for both body and vehicular blockage in [6]. This explicit version can lead to a substantial complexity in 5G-NR system/link level studies. Further, this explicit version critically relies on the DKED model, whose efficacy in capturing loss in the human body blockage case needs further attention as illustrated by the slight mismatch between simulation-based and measurement studies.

TABLE VI
PROPOSED STATISTICAL MODEL FOR DYNAMIC BLOCKAGE

Blocker index	ϕ_k	x_k	θ_k	y_k	Blockage loss (in dB)
$k = 2, 3, 4, 5$ (Human)	$\mathcal{U}([0^\circ, 360^\circ))$	2.5°	90°	15°	Low-complexity: $\mathcal{N}(\mu = 8.5 \text{ dB}, \sigma = 2.5 \text{ dB})$ High-complexity: Gaussian-Weibull mixture with $p_1 = 0.15$, $\mu = 9.5$, $\sigma = 1.95$, $p_2 = 0.85$, $\alpha = 9.4$, and $\beta = 3.7$
$k = 6, 7, 8$ (Vehicular)	$\mathcal{U}([0^\circ, 360^\circ))$	15°	90°	5°	Simulations-based: $\mathcal{N}(\mu = 12 \text{ dB}, \sigma = 1.5 \text{ dB})$

IV. TIME-SCALES OF BLOCKAGE EVENTS

Understanding the time-scales at which blockage events happen can help us mitigate these disruptions in terms of signal quality degradation and even possible link losses. It is important to note that these time-scales are determined by the dynamics of blockage, and in particular, the speed at which humans walk (or other blockers emerge and depart) to block a link or the speed at which the hand grabs the UE and blocks the link. Towards this goal, we define the *link degradation time* as the time required for the RSSI to drop from the steady-state value to its minima in the case of a good-to-moderate channel condition, or the time required for the RSSI to drop from the steady-state value to a complete link loss in the case of a poor channel condition. With this definition, the link degradation time serves as the worst-case time by which a beam switching/link adaptation procedure must be enabled to ensure that mmW coverage remains robust, reliable and seamless.

To understand the scope of link degradation and time-scales of blockage events, six experiments are performed with the experimental prototype described in Sec. II-B. The prototype uses

a proprietary transmission frame structure where each sub-frame is 125 μ s. Analog beamforming with proprietary directional codebooks (see design principles in [16], [23]) is implemented at both the base-station and UE ends. These codebooks correspond to testing the link over 16 transmit side beams and 20 UE side beams (5 beams over four subarrays) for a beam scanning periodicity/latency of 40 ms. Thus, any link degradation/loss can be estimated to within an accuracy of ± 20 ms. The first four of these six experiments correspond to link degradation due to dynamic blockage (humans walking around near the UE) and the last two experiments correspond to self-blockage (the use of the hand). Each experiment corresponds to different link/channel conditions with multiple independent tests performed in these settings. More details on these experiments including the number of tests are provided in Table VII.

Figs. 6(a)-(b) capture the CDF of link degradation time across different channel conditions with human body blockage and self-blockage, respectively. The CDFs from the true data are presented with solid lines and piecewise linear estimated fits (across adjacent sample points) are presented with dashed lines. From these plots, we note that the link degradation time generally decreases as the channel condition deteriorates with no substantial difference between hand and body blockage dynamics. Thus these plots suggest that the time-scales at which blockages are observed at the UE end are indicative of physical movements (of either humans or the hand) which can be on the order of a few 100s of ms (or slower). Thus, from Fig. 6, it is not surprising to see that the median value of link degradation time being on the order of 200-480 ms for body blockage and 240 ms for hand blockage. Given the sub-ms latencies for beam switching possible in 5G-NR, these estimates suggest that blockage events can be handled with a robust beam management procedure.

V. SOLUTIONS TO COMBAT BLOCKAGE

Multiple solutions can either be individually/jointly considered to handle the deleterious impact of performance degradation with blockage.

- Network densification: Beamforming design for mmW systems is expected to leverage *directional* solution structures due to their robustness with different beamforming architectures and their implementation ease [16], [17], [36]. Thus, both the base-station and the UE are expected to steer their beams towards the dominant clusters in the channel and blockage in these directions can significantly deteriorate the performance of mmW systems.

TABLE VII

DESCRIPTION OF LINK DEGRADATION EXPERIMENTS

Experiment	Blockage type	Channel condition	Number of tests
1	Body	Good	36
2	Body	Good-to-medium	32
3	Body	Medium	44
4	Body	Poor	39
5	Hand	Poor	38
6	Hand	Good	34

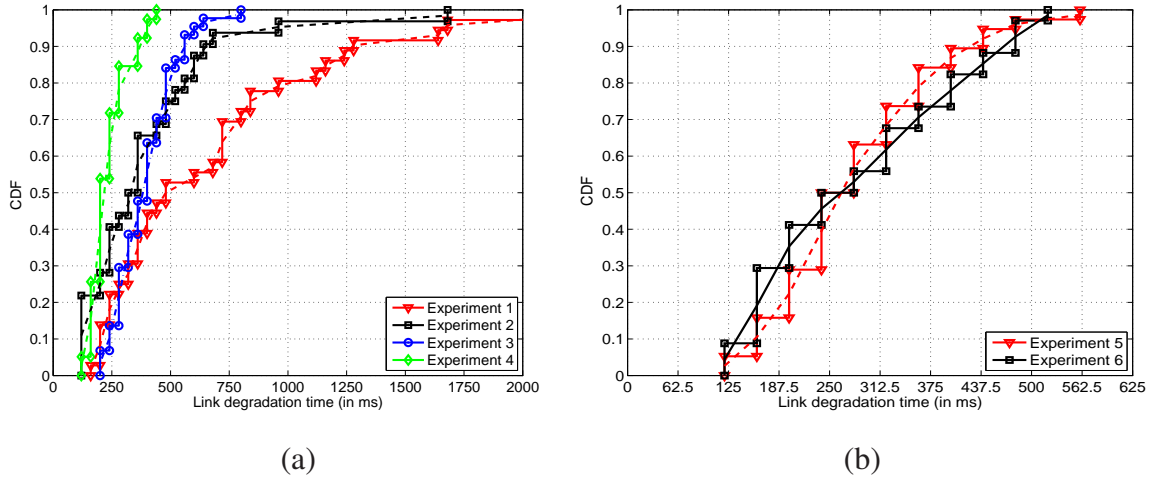


Fig. 6. CDF of link degradation time for (a) body blockage and (b) hand blockage experiments.

In this context, densifying the network with overlap in coverage across multiple cells [3] can provide higher fade margins to prevent link losses in mmW deployments. Further, the deployment of multiple base-stations could lead to the feasibility of different/distinct dominant paths from these base-stations to a certain UE via distinct reflectors, scatterers or clusters thereby reducing the risk of dramatic link degradations/failures due to blockage.

- Subarray switching: Subarray diversity is critical at the UE end due to the reduced spatial/angular coverage possible with an antenna at mmW frequencies relative to sub-6 GHz frequencies. For example, the typical angular coverage with a dipole/patch antenna is

on the order of 90° to 120° implying the necessity of multiple subarrays as well as a careful selection¹² of the locations of these subarrays for full spherical coverage. Thus, coverage over the sphere is realized in a form-factor UE design with distinct subarrays corresponding to distinct clusters in the channel environment. This fact can be leveraged by allowing/enabling a subarray switching procedure via beam management before an established link degrades significantly.

In this context, mmW measurements reported in [37] for indoor environments (office and shopping mall) suggest that (on average) 4-5 distinct clusters corresponding to distinct directions appear to be within a power differential of 5 dB of each other implying a reasonable level of path diversity for indoor mmW deployments. Similarly, in outdoor mobility tests with the prototype reported in [23, Sec. IV], inter-base-station beam switching and handover are shown to be both feasible and important with blockages from static geographical/topographical blockages/features, foliage, etc.

- Fall back mechanisms: With the above background, there could also be scenarios where the network is not densified sufficiently or the channel environment is sparse ensuring that there are no better clusters to switch to. In these scenarios, the UE is left with little choice but to continue to use the degraded link with some codebook enhancements (possibly proprietary from an implementation standpoint). These enhancements could help improve the array gain seen at the UE side by performing a maximum ratio combining of the effective channel corresponding to the true channel and the near-field effects of the hand. Alternately, the UE could consider fall back to legacy carriers (such as 4G/LTE) or 5G-NR carriers such as those at sub-6 GHz frequencies.

VI. CONCLUDING REMARKS

Given the prospects of accelerated deployment of 5G-NR systems, there has been an emerging interest on a number of issues that need to be addressed to make these systems technically viable and commercially profitable [28], [29]. The focus of this work is on one such aspect: blockage of mmW signals due to the user itself (hand or body parts) as well as humans or vehicles in

¹²The constraints associated with the location of camera(s), speaker, microphone, sensors, etc. lead to a careful optimization of the location of antennas in a form-factor UE design (see, e.g., Fig. 1).

the vicinity of the UE. To the best of our knowledge, the impact of blockage as well as their implications in terms of PHY layer mechanisms to ameliorate their impact have not been reported for 28 or 60 GHz systems (two important use-cases of 5G-NR), especially with form-factor UE designs.

In this context, our studies at 28 and 60 GHz show that large parts of the spatial/angular coverage area can be blocked by the hand. This is because the user's hand and body serve as primary obstacles in obscuring the radiation coverage of the UE antennas with the size of the hand being large relative to the UE. We also report measurement-driven studies of loss due to self-blockage with a 28 GHz experimental prototype. Our studies show that in contrast to prior reports of 30 to 40 dB blockage losses, even a hard hand grip with form-factor UEs could see significantly lower losses in the range of 5 to 20 dB (with a median loss of 15 dB). These discrepancies arise because of the beamwidth differences between prior studies that are based on horn antenna measurements (much smaller beamwidths) relative to form-factor phased arrays (that could have larger beamwidths). These relative beamwidth differences allow much higher signal energies to be radiated/captured in form-factor UEs. In the more optimistic scenario of looser hand grips with gap between fingers, some antenna elements can radiate/capture signal energy through the air gaps leading to even further reduced blockage losses.

We also propose a simulation methodology for capturing the impact of dynamic (human and vehicular) blockers in the vicinity of the UE. The spatial/angular coverage lost is studied and the DKED model is used to estimate the loss due to the blockers. Comparisons with measurement data of the blockage loss with human blockers in an indoor office setting shows a reasonable first-order fit with the data from the proposed simulation methodology. Given the difficulties in obtaining measurement-based estimates for loss with vehicular blockers in outdoor deployments, the proposed simulation framework could serve as a reasonable substitute for system level studies. In this context, the proposed simulation methodology as well as the statistical model generated from the data has already had some far-reaching impact on channel modeling at 3GPP. In particular, Option A of the blockage model in the 3GPP Rel. 14 channel modeling document [6, pp. 53-55] is based on ideas expounded in this paper.

Another contribution of this work is in terms of understanding the time-scales at which blockage events and their disruptions can be seen to impact the UE side. Based on experiments with the 28 GHz prototype, we show that these blockage events can be attributed to physical

movements and the time-scales at which these disruptions happen are on the order of a few 100 ms (or more). These estimates offer insights into the feasibility of mitigation mechanisms to address blockage impairments. Given a rich channel environment, network densification (as seen from the base-station perspective) or the use of multiple subarrays (as seen from the UE perspective) can help given that the 5G-NR standard allows sub-ms (or a few ms) effective latencies in beam/subarray switching. In the case of a sparse channel environment (e.g., rural settings, highways, etc.), mitigation mechanisms could be fall back on to legacy carriers or proprietary codebook enhancements (on top of the steady-state beamforming codebooks used at the UE end). The design of PHY layer enhancements to realize these ways forward could be the subject of interesting future work in this area.

APPENDIX

A. Parameter Learning for a Gaussian Mixture Model

Let $\Phi_{\theta_1}(y)$ and $\Phi_{\theta_2}(y)$ denote the density functions of the two Gaussians in the mixture corresponding to parameters $\theta_i = \{\mu_i, \sigma_i\}$, $i = 1, 2$. That is,

$$\Phi_{\theta_i}(y) = \frac{1}{\sqrt{2\pi\sigma_i^2}} \cdot e^{-\frac{(y-\mu_i)^2}{2\sigma_i^2}}, \quad -\infty < y < \infty$$

with the mixture model corresponding to a mixture probability p_1 given as

$$\Phi_{\theta}(y) = \frac{p_1}{\sqrt{2\pi\sigma_1^2}} \cdot e^{-\frac{(y-\mu_1)^2}{2\sigma_1^2}} + \frac{(1-p_1)}{\sqrt{2\pi\sigma_2^2}} \cdot e^{-\frac{(y-\mu_2)^2}{2\sigma_2^2}}.$$

We use \mathcal{L} to denote the log likelihood function for the data (denoted as y_i , $i = 1, \dots, N$) and an unobserved latent variable, $\Delta_i \in \{0, 1\}$. The observation y_i comes from Model 1 (captured by θ_1) if $\Delta_i = 0$, or from Model 2 (captured by θ_2) if $\Delta_i = 1$. This log likelihood function is given as

$$\mathcal{L} = \sum_{i=1}^N \left[(1 - \Delta_i) \log(\Phi_{\theta_1}(y_i)) + \Delta_i \log(\Phi_{\theta_2}(y_i)) \right] + \sum_{i=1}^N \left[(1 - \Delta_i) \log(1 - \pi) + \Delta_i \log(\pi) \right]$$

where π denotes $P(\Delta_i = 1)$. Since we do not know Δ_i , we replace it with its conditional expectation:

$$\gamma_i(\theta) = \mathbf{E} \left[\Delta_i | \theta, \{y_j\} \right] = P(\Delta_i = 1 | \theta, \{y_j\})$$

and perform the Expectation Maximization algorithm for learning the parameters [38, 8.5.1, pp. 272-275 and Algorithm 8.1]. To keep this paper self-contained, we provide the parameter

learning algorithm corresponding to stopping at k_{\max} iterations below. The choice of k_{\max} is determined by an *a priori* choice of based on a stopping criterion.

Algorithm 1 (Parameter learning for a Gaussian mixture model)

For $k = 1$, initialize $\hat{p}_{1,1} = 0.5$, $\hat{\mu}_{1,1} = \min_i y_i$, $\hat{\mu}_{2,1} = \max_i y_i$, $\bar{y} = \frac{\sum_i y_i}{N}$, $\hat{\sigma}_{1,1}^2 = \hat{\sigma}_{2,1}^2 = \frac{1}{N} \sum_i (y_i - \bar{y})^2$.

for all $k = 1, \dots, k_{\max} - 1$ **do**

$$\text{Define } \hat{\gamma}_i = \frac{\frac{\hat{p}_{1,k}}{\sqrt{2\pi\hat{\sigma}_{1,k}^2}} \times \exp\left(-\frac{(y_i - \hat{\mu}_{1,k})^2}{2\hat{\sigma}_{1,k}^2}\right)}{\frac{\hat{p}_{1,k}}{\sqrt{2\pi\hat{\sigma}_{1,k}^2}} \times \exp\left(-\frac{(y_i - \hat{\mu}_{1,k})^2}{2\hat{\sigma}_{1,k}^2}\right) + \frac{\hat{p}_{2,k}}{\sqrt{2\pi\hat{\sigma}_{2,k}^2}} \times \exp\left(-\frac{(y_i - \hat{\mu}_{2,k})^2}{2\hat{\sigma}_{2,k}^2}\right)} \text{ for } i = 1, \dots, N.$$

Update $\hat{\mu}_{1,k+1}$ and $\hat{\mu}_{2,k+1}$ with $\frac{\sum_i \hat{\gamma}_i y_i}{\sum_i \hat{\gamma}_i}$ and $\frac{\sum_i (1 - \hat{\gamma}_i) y_i}{\sum_i (1 - \hat{\gamma}_i)}$, respectively.

Update $\hat{\sigma}_{1,k+1}^2$ and $\hat{\sigma}_{2,k+1}^2$ with $\frac{\sum_i \hat{\gamma}_i (y_i - \hat{\mu}_{1,k+1})^2}{\sum_i \hat{\gamma}_i}$ and $\frac{\sum_i (1 - \hat{\gamma}_i) (y_i - \hat{\mu}_{2,k+1})^2}{\sum_i (1 - \hat{\gamma}_i)}$, respectively.

Update $\hat{p}_{1,k+1}$ with $\frac{\sum_i \hat{\gamma}_i}{N}$.

end for

□

REFERENCES

- [1] V. Raghavan, T. Bai, A. Sampath, O. H. Koymen, and J. Li, "Modeling and combating blockage in millimeter wave systems," *Submitted to IEEE International Workshop on Signal Processing Advances in Wireless Communications (SPAWC), Kalamata, Greece*, June 2018.
- [2] F. Khan and Z. Pi, "An introduction to millimeter wave mobile broadband systems," *IEEE Commun. Magaz.*, vol. 49, no. 6, pp. 101–107, June 2011.
- [3] N. Bhushan, J. Li, D. Malladi, R. Gilmore, D. Brenner, A. Damnjanovic, R. T. Sukhasvi, C. Patel, and S. Geirhofer, "Network densification: The dominant theme for wireless evolution into 5G," *IEEE Commun. Magaz.*, vol. 52, no. 2, pp. 82–89, Feb. 2014.
- [4] T. S. Rappaport, S. Sun, R. Mayzus, H. Zhao, Y. Azar, K. Wang, G. N. Wong, J. K. Schulz, M. K. Samimi, and F. Gutierrez, "Millimeter wave mobile communications for 5G cellular: It will work!," *IEEE Access*, vol. 1, pp. 335–349, 2013.
- [5] F. Boccardi, R. W. Heath, Jr., A. Lozano, T. L. Marzetta, and P. Popovski, "Five disruptive technology directions for 5G," *IEEE Commun. Magaz.*, vol. 52, no. 2, pp. 74–80, Feb. 2014.
- [6] 3GPP TR 38.901 V14.2.0 (2017-09), "Technical Specification Group Radio Access Network; Study on Channel Model for Frequencies from 0.5 to 100 GHz (Rel. 14)," Sept. 2017.
- [7] Aalto University, AT&T, BUPT, CMCC, Ericsson, Huawei, Intel, KT Corporation, Nokia, NTT DOCOMO, NYU, Qualcomm, Samsung, U. Bristol, and USC, "White paper on '5G channel model for bands up to 100 GHz,'" v2.3, Oct. 2016, Available: [Online]. <http://www.5gworkshops.com/5GCM.html>.

- [8] A. Maltsev et al., “Channel models for 60 GHz WLAN systems, doc: IEEE 802.11-09/0334r8,” 2010, Available: [Online]. <https://mentor.ieee.org/802.11/documents>.
- [9] METIS 2020, “METIS channel model, Deliverable D1.4v3,” July 2015, Available: [Online]. https://www.metis2020.com/wp-content/uploads/deliverables/METIS_D1.4_v3.pdf.
- [10] V. Raghavan, A. Partyka, L. Akhondzadeh-Asl, M. A. Tassoudji, O. H. Koymen, and J. Sanelli, “Millimeter wave channel measurements and implications for PHY layer design,” *IEEE Trans. Ant. Propagat.*, vol. 65, no. 12, pp. 6521–6533, Dec. 2017.
- [11] F. Rusek, D. Persson, B. K. Lau, E. G. Larsson, T. L. Marzetta, O. Edfors, and F. Tufvesson, “Scaling up MIMO: Opportunities and challenges with very large arrays,” *IEEE Sig. Proc. Magaz.*, vol. 30, no. 1, pp. 40–60, Jan. 2013.
- [12] S. Hur, T. Kim, D. J. Love, J. V. Krogmeier, T. A. Thomas, and A. Ghosh, “Millimeter wave beamforming for wireless backhaul and access in small cell networks,” *IEEE Trans. Commun.*, vol. 61, no. 10, pp. 4391–4403, Oct. 2014.
- [13] S. Sun, T. S. Rappaport, R. W. Heath, Jr., A. Nix, and S. Rangan, “MIMO for millimeter wave wireless communications: Beamforming, spatial multiplexing, or both?,” *IEEE Commun. Magaz.*, vol. 52, no. 12, pp. 110–121, Dec. 2014.
- [14] J. Brady, N. Behdad, and A. M. Sayeed, “Beamspace MIMO for millimeter-wave communications: System architecture, modeling, analysis and measurements,” *IEEE Trans. Ant. Propagat.*, vol. 61, no. 7, pp. 3814–3827, July 2013.
- [15] O. El Ayach, S. Rajagopal, S. Abu-Surra, Z. Pi, and R. W. Heath, Jr., “Spatially sparse precoding in millimeter wave MIMO systems,” *IEEE Trans. Wireless Commun.*, vol. 13, no. 3, pp. 1499–1513, Mar. 2014.
- [16] V. Raghavan, J. Cezanne, S. Subramanian, A. Sampath, and O. H. Koymen, “Beamforming tradeoffs for initial UE discovery in millimeter-wave MIMO systems,” *IEEE Journ. Sel. Topics in Sig. Proc.*, vol. 10, no. 3, pp. 543–559, Apr. 2016.
- [17] V. Raghavan, S. Subramanian, J. Cezanne, A. Sampath, O. H. Koymen, and J. Li, “Single-user vs. multi-user precoding for millimeter wave MIMO systems,” *IEEE Journ. Sel. Areas in Commun.*, vol. 35, no. 6, pp. 1387–1401, June 2017.
- [18] C. A. Balanis, *Antenna Theory: Analysis and Design*, Wiley-Interscience, 3rd edition, 2005.
- [19] Federal Communications Commission, “FCC takes steps to facilitate mobile broadband and next generation wireless technologies in spectrum above 24 GHz,” July 2016, Available: [Online]. <https://www.fcc.gov/document/fcc-adopts-rules-facilitate-next-generation-wireless-technologies>.
- [20] W. Roh, J.-Y. Seol, J. Park, B. Lee, J. Lee, Y. Kim, J. Cho, K. Cheun, and F. Aryanfar, “Millimeter-wave beamforming as an enabling technology for 5G cellular communications: Theoretical feasibility and prototype results,” *IEEE Commun. Magaz.*, vol. 52, no. 2, pp. 106–113, Feb. 2014.
- [21] S. Rangan, T. S. Rappaport, and E. Erkip, “Millimeter wave cellular networks: Potentials and challenges,” *Proc. IEEE*, vol. 102, no. 3, pp. 366–385, Mar. 2014.
- [22] A. Ghosh, T. A. Thomas, M. C. Cudak, R. Ratasuk, P. Moorut, F. W. Vook, T. S. Rappaport, G. R. MacCartney, Jr., S. Sun, and S. Nie, “Millimeter-wave enhanced local area systems: A high data-rate approach for future wireless networks,” *IEEE Journ. Sel. Areas in Commun.*, vol. 32, no. 6, pp. 1152–1163, June 2014.
- [23] V. Raghavan, A. Partyka, S. Subramanian, A. Sampath, O. H. Koymen, K. Ravid, J. Cezanne, K. K. Mukkavilli, and J. Li, “Millimeter wave MIMO prototype: Measurements and experimental results,” *IEEE Commun. Magaz. (In print)*, Jan. 2018.
- [24] M. Peter, M. Wisotzki, M. Raceala-Motoc, W. Keusgen, R. Felbecker, M. Jacob, S. Priebe, and T. Kuerner, “Analyzing human body shadowing at 60 GHz: Systematic wideband MIMO measurements and modeling approaches,” *Proc. European Conf. Ant. and Propagat.*, pp. 468–472, Mar. 2012.

- [25] G. R. MacCartney, Jr., S. Deng, S. Sun, and T. S. Rappaport, "Millimeter-wave human blockage at 73 GHz with a simple double knife-edge diffraction model and extension for directional antennas," *Proc. IEEE Veh. Tech. Conf. (Fall), Montreal, Canada*, pp. 1–6, Sept. 2016.
- [26] G. R. MacCartney, Jr. and T. S. Rappaport, "A flexible millimeter-wave channel sounder with absolute timing," *IEEE Journ. Sel. Areas in Commun.*, vol. 35, no. 6, pp. 1402–1418, June 2017.
- [27] K. Zhao, J. Helander, Z. Ying, D. Sjöberg, M. Gustafsson, and S. He, "mmWave phased array in mobile terminal for 5G mobile system with consideration of hand effect," *Proc. IEEE Veh. Tech. Conf. (Spring), Glasgow, Scotland*, pp. 1–4, May 2015.
- [28] W. Hong, K-H. Baek, and S. Ko, "Millimeter-wave 5G antennas for smartphones: Overview and experimental demonstration," *IEEE Trans. Ant. Propagat.*, vol. 65, no. 12, pp. 6250–6261, Dec. 2017.
- [29] W. Hong, Z. H. Jiang, C. Yu, J. Zhou, P. Chen, Z. Yu, H. Zhang, B. Yang, X. Pang, M. Jiang, Cheng Y, M. K. T. Al-Nuaimi, Y. Zhang, J. Chen, and S. He, "Multibeam antenna technologies for 5G wireless communications," *IEEE Trans. Ant. Propagat.*, vol. 65, no. 12, pp. 6231–6249, Dec. 2017.
- [30] D. Andreuccetti, R. Fossi, and C. Petrucci, "An Internet resource for the calculation of the dielectric properties of body tissues in the frequency range 10 Hz - 100 GHz (Based on data published by C. Gabriel et al. in 1996)," *IFAC-CNR, Florence (Italy)*, 1997, Available: [Online]. <http://niremf.ifac.cnr.it/tissprop/>.
- [31] N. Chahat, M. Zhadobov, R. Augustine, and R. Sauleau, "Human skin permittivity models for millimeter-wave range," *Electronics Lett.*, vol. 47, no. 7, pp. 427–428, Mar. 2011.
- [32] C. Gabriel, S. Gabriel, and E. Corthout, "The dielectric properties of biological tissues: I. Literature survey," *Physics in Medicine and Biology*, vol. 41, no. 11, pp. 2231–2249, 1996.
- [33] J. D. Gibbons and S. Chakraborti, *Nonparametric Statistical Inference*, Chapman & Hall/CRC Press, 5th edition, 2011.
- [34] R. G. Kouyoumjian and P. H. Pathak, "A uniform geometrical theory of diffraction for an edge in a perfectly conducting surface," *Proc. IEEE*, vol. 62, no. 11, pp. 1448–1461, Nov. 1974.
- [35] P. H. Pathak, W. Burnside, and R. Marhefka, "A uniform GTD analysis of the diffraction of electromagnetic waves by a smooth convex surface," *IEEE Trans. Ant. Propagat.*, vol. 28, no. 5, pp. 631–642, May 1980.
- [36] V. Raghavan, S. Subramanian, J. Cezanne, and A. Sampath, "Directional beamforming for millimeter-wave MIMO systems," *Proc. IEEE Global Telecommun. Conf., San Diego, CA*, pp. 1–7, Dec. 2015.
- [37] Qualcomm, "Clustering methodology and results based on omni-directional and azimuthal scans in 29 and 61 GHz," *R1-161666, 3GPP TSG RAN WG1 #AH Channel Model, Ljubljana, Slovenia*, Mar. 2016.
- [38] T. Hastie, R. Tibshirani, and J. Friedman, *The Elements of Statistical Learning*, Springer, USA, 2nd edition, 2008.